Multi-scale structuring of cell-instructive cellulose nanocrystal composite hydrogel sheets via sequential electrospinning and thermal wrinkling

Kevin J. De France [a,b,], Fei Xu [b], Samaneh Toufanian [b], Katelyn J. W. Chan [b], Somiraa Said [b], Taylor C. Stimpson [b], Eduardo González-Martínez [c], Jose M. Moran-Mirabal [c], Emily D. Cranston [d,e], and Todd Hoare [b,f,]**

- *a. Laboratory of Cellulose & Wood Materials, Empa – Swiss Federal Laboratories for Materials Science and Technology, Überlandstrasse 129, 8600 Dübendorf, Switzerland*
- *b. Department of Chemical Engineering, McMaster University, 1280 Main Street West, Hamilton, ON L8S 4L8, Canada*
- *c. Department of Chemistry and Chemical Biology, McMaster University, 1280 Main Street West, Hamilton, ON L8S 4M1, Canada*
- *d. Department of Wood Science, University of British Columbia, 2424 Main Mall, Vancouver, BC, V6T 1Z4, Canada*
- *e. Department of Chemical and Biological Engineering, University of British Columbia, 2360 East Mall, Vancouver, BC V6T 1Z3, Canada*
- *f. School of Biomedical Engineering, McMaster University, 1280 Main Street West, Hamilton, ON L8S 4L8, Canada*

* Corresponding author emails
Kevin J. De France: kevin.defrance@empa.ch
Todd Hoare: hoaretr@mcmaster.ca

This document is the accepted manuscript version of the following article:
De France, K. J., Xu, F., Toufanian, S., Chan, K. J. W., Said, S., Stimpson, T. C., … Hoare, T. (2021). Multi-scale structuring of cell-instructive cellulose nanocrystal composite hydrogel sheets via sequential electrospinning and thermal wrinkling. Acta Biomaterialia. https://doi.org/10.1016/j.actbio.2021.04.044

Abstract

Structured hydrogel sheets offer the potential to mimic the mechanics and morphology of native cell environments *in vitro*; however, controlling the morphology of such sheets across multiple length scales to give cells consistent multi-dimensional cues remains challenging. Here, we demonstrate a simple two-step process based on sequential electrospinning and thermal wrinkling to create nanocomposite poly(oligoethylene glycol methacrylate)/cellulose nanocrystal hydrogel sheets with a highly tunable multi-scale wrinkled (micro) and fibrous (nano) morphology. By varying the time of electrospinning, rotation speed of the collector, and geometry of the thermal wrinkling process, the hydrogel nanofiber density, fiber alignment, and wrinkle geometry (biaxial or uniaxial) can be independently controlled. Adhered C2C12 mouse myoblast muscle cells display a random orientation on biaxially wrinkled sheets but an extended morphology (directed preferentially along the wrinkles) on uniaxially wrinkled sheets. While the nanofiber orientation had a smaller effect on cell alignment, parallel nanofibers promoted improved cell alignment along the wrinkle direction while perpendicular nanofibers disrupted alignment. The highly tunable structures demonstrated are some of the most complex morphologies engineered into hydrogels to-date without requiring intensive micro/nanofabrication approaches and offer the potential to precisely regulate cell-substrate interactions in a "2.5D" environment (i.e. a surface with both micro- and nano-structured topographies) for *in vitro* cell screening or *in vivo* tissue regeneration.

Keywords: cellulose nanocrystals, hierarchical hydrogel structuring, electrospinning, thermal wrinkling, cell-biomaterial interactions

1. Introduction

Hydrogels that mimic the structural and physiological properties of the native extracellular matrix (ECM) offer potential to both expand our understanding of cell-matrix interactions *in vitro* and improve our capacity to regenerate tissues using synthetic scaffolds *in vivo*.[1] In particular, given that many tissues are hierarchically structured in nature, developing methods to structure hydrogels on multiple length scales is essential to improve our capacity to mimic native ECM structures. This would improve the performance of such hydrogels in probing fundamental cell-matrix interactions, encapsulating cells for therapeutic delivery, and designing scaffolds for tissue engineering.[2–6] Common methods to prepare 3D structured hydrogels typically focus on using a template to control the morphology of the surrounding hydrogel, including salt/porogen templating,[7] bicontinuous emulsion templating,[8] gas foaming,[9] and cryogelation,[10] although other template-free techniques including 3D printing[11] and electrospinning[12] have also been used. However, all these methods have limitations in terms of their capacity to create structures with adequate resolution and/or hierarchical/multi-scale structures commensurate in size with the features of the native ECM. More precise patterns can be achieved using microcontact printing,[13–16] soft embossing/contact lithography,[17–20] and photolithography;[21–24] however, these 2D techniques cannot fully reproduce the 3D cell environments of native ECM. As such, new strategies are required to facilitate controllable multi-scale structuring of hydrogels with the length scale and dimensionality required for precise ECM mimicry.

In order to overcome these limitations, we have recently demonstrated a technique based on thermal wrinkling to prepare structured thin film hydrogels in “2.5D” (i.e. thin films with micro/nanoscale topologies in the z-direction) composed of hydrazone-crosslinked poly(oligoethylene glycol methacrylate) (POEGMA) and cellulose nanocrystals (CNCs),[25] both of which have been extensively researched for their use in biomedical applications given the *in vivo* tolerability, ease of functionalization, and minimally invasive delivery of the *in*

situ-gelling POEGMA component[26–30] and the low cytotoxicity, high strength, tunable surface chemistry, and commercial availability of the CNC component;[30–37] of note, alignment of the anisotropic CNCs using shear or magnetic forces has also been demonstrated to promote cell orientation.[38–40] While several previous studies have utilized buckling or wrinkling approaches to explore the effects of the length scale of wrinkled structures on a variety of substrates for cell orientation/contact guidance,[41–45] the inherent restrictions on feature size via wrinkling-based techniques (which are directly correlated to the elasticity and thickness of the wrinkling layer) make it difficult to simulate the dual nanofibrous/macroporous structure of native ECM and thus necessitate the development of improved/novel preparation techniques.

Electrospinning is a versatile and attractive method of creating nanofibers of tunable properties by changing process parameters such as the flow rate, voltage, and tip-to-collector distance.[46] The nanofibrous nature of electrospun mats makes them prime candidates to be used as cell scaffolds given the presence of similar nanofibrous structures in native ECM.[47–49] Although electrospinning is commonly used in tissue engineering to create nanofibrous networks of water insoluble but degradable polymers,[46] the technical challenge associated with achieving gelation on an appropriate time scale to facilitate electrospinning while maintaining the nanofibrous structure at the collector have limited the use of electrospinning for creating hydrogel-based scaffolds. Furthermore, most previously-reported techniques use heat or light-induced free radical crosslinking to form the hydrogel network during electrospinning, which may result in cytotoxicity or necessitate additional processing/purification steps.[12] We have recently reported the potential to form nanofibrous hydrogels without the need for UV irradiation or small-molecule chemical crosslinking using an all-aqueous reactive extrusion process in which POEGMA oligomers functionalized with kinetically bio-orthogonal aldehyde (A-POEGMA) and hydrazide (H-POEGMA) moieties are co-electrospun from a double barrel syringe.[12,47] While the starting materials are non-

viscous, the rapid hydrazone crosslinking achieved upon mixing (and accelerated as water evaporates following jet formation) enables the formation of well-defined and tunable hydrogel nanofibers in the presence of live cells.[12,47] Alignment of the nanofibers can be achieved using a rotating collector, with the resulting oriented scaffolds having demonstrated capacity for effectively orienting C2C12 muscle cells as compared to non-patterned controls.[49–53] However, there is relatively little research focused on controlling electrospun mat morphology in a hierarchical manner to better mimic the complex hierarchical morphology of native ECM. Furthermore, research aimed at modelling the interactions between cells and substrates typically focuses solely on substrate topography on the nanoscale[46] or on the microscale[43] rather than integrating cues on multiple length scales, as per the native ECM.

We have previously demonstrated that the strong intermolecular interactions between CNCs and POEGMA can enable the formation of mechanically strong and structured hydrogels.[40,54–57] Herein, by leveraging these interactions, we use a combination of electrospinning and thermal wrinkling to fabricate hierarchically-structured “2.5D” hydrogel sheets. More specifically, we demonstrate that POEGMA-CNC composite hydrogel sheets with tunable morphologies across multiple length scales can be produced by electrospinning a mat of randomly oriented or uniaxially aligned nanofibers on a thin hydrogel base layer and subsequently performing a thermal wrinkling process to create underlying biaxial or uniaxial wrinkles in a preferred direction. Such hierarchical morphologies are shown to provide multi-scale and multi-morphological cues to control both cell adhesion and cell orientation on the hydrogel sheet, offering new potential for directing cell behavior using “2.5D” cell scaffolds that can provide the cell adhesion/directionality cues of 3D tissues coupled with the significantly easier imaging enabled by conventional 2D cell constructs.

2. Materials and Methods

2.1 Materials

Oligo(ethylene glycol) methyl ether methacrylate ($OEGMA_{500}$, Sigma-Aldrich, 95%) was purified in a column of basic aluminum oxide prior to use. N-(2,2-dimethoxyethyl)-methacrylamide (DMAEAm) was synthesized as previously described.[26] Acrylic acid (AA, Sigma-Alrich, 99%), 2,2-azobisisobutyric acid dimethyl ester (AIBMe, Wako Chemicals, 98.5%), adipic acid dihydrazide (ADH, Alfa Aesar, 98%), N'-ethyl-N-(3-(dimethylamino)-propyl)-carbodiimide (EDC, Carbosynth, Compton CA, commercial grade), thioglycolic acid (TGA, Sigma-Aldrich, 98%), sodium hydroxide (EMD Millipore Germany), sodium chloride (Sigma-Aldrich, ≥ 99.5%), hydrochloric acid (LabChem Inc., 1M), dioxane (Caledon Laboratory Chemicals, reagent grade), sulfuric acid (Sigma-Aldrich, 95-98%), Whatman cotton filter paper (cat. No. 1703-050, GE Healthcare Canada), high molecular weight poly(ethylene oxide) (PEO, 600 kDa, Sigma-Aldrich), bovine serum albumin (BSA, Sigma Aldrich, >96%), fluorescein isothiocyanate (FITC, Sigma Aldrich, 90%), carboxyfluorescein diacetate succinimidyl ester (Vybrant® CFDA SE Cell Tracer Kit, Invitrogen), 4′,6-diamidino-2-phenylindole (DAPI nuclear staining kit, Invitrogen), and methyltrichlorosilane (MTS cell proliferation colorimetric assay kit, BioVision) were all used as received. C2C12 *Mus musculus* mouse myoblast cells (ATCC: Cedarlane Laboratories, Burlington, ON) were cultured in Dulbecco's modified Eagle medium (DMEM) supplemented with 10 % fetal bovine serum (FBS) and 1% penicillin streptomycin (PS) according to manufacturer recommended protocols. Millipore Milli-Q grade distilled deionized water (DIW, resistivity > 18.2 MΩ cm) and phosphate buffered saline (PBS, 10mM, BioShop) were used as indicated.

2.2 Synthesis of Hydrazide and Aldehyde Functionalized POEGMA Copolymers

POEGMA copolymers were synthesized to have 30 mol% hydrazide or aldehyde functional groups following our previously described protocol.[26] For the hydrazide POEGMA precursor (H-POEGMA), AIBMe (74 mg), $OEGMA_{500}$ (8.0 g), AA (550 µL), and TGA (150 µL, 10 wt% in dioxane) were added to a 250 mL round-bottom flask. For the aldehyde POEGMA precursor (A-POEGMA), AIBMe (100 mg), $OEGMA_{500}$ (8.0 g), DMAEAm (1.2 g), and TGA (20 µL, 10 wt% in dioxane) were added to a separate 250 mL round-bottom flask. 40 mL of dioxane was then added to each flask prior to purging with nitrogen for 20 min. Polymerization was conducted at 75 °C for 4 hours, after which the flasks were allowed to cool overnight. Following solvent evaporation, 200 mL of DIW, ADH (8.66 g) and EDC (3.87 g) were added to the H-POEGMA solution and the pH was maintained at 4.75 ± 0.1 for 4 hours via dropwise addition of 1 M HCl to functionalize the pre-polymer with hydrazide groups. In parallel, 200 mL of 0.33 M HCl was added to the A-POEGMA solution and stirred for 16 hours at room temperature to hydrolyze the diacetal groups to aldehyde groups. The resulting functional polymers were dialyzed (MWCO = 3500 g/mol) in DIW over 6 × 6 hr (minimum) cycles and subsequently lyophilized to dryness. The obtained POEGMA copolymers were diluted to 20 wt% in DIW and stored at 4 °C prior to use.

Aqueous size exclusion chromatography was performed using a Waters 515 HPLC pump, Waters 717 Plus autosampler, three Ultrahydrogel columns (30 cm x 7.8 mm i.d.; exclusion limits of 0–3 kDa, 0–50 kDa and 2–300 kDa), a Waters 2414 refractive index detector, and a mobile phase consisting of 25 mM N-cyclohexyl-2-aminoethanesulfonic acid (CHES) buffer, 500 mM $NaNO_3$ and 10 mM NaN_3 at a flow rate of 0.8 mL min^{-1}. The system was calibrated with narrow-dispersed PEG standards (106 to 584 x 10^3 g mol^{-1}), yielding molecular weights and dispersities of 17.2 kDa and 3.8 for A-POEGMA and 18.0 kDa and 2.8 for H-POEGMA respectively. The degree of aldehyde functionalization of A-POEGMA (26.6 mol%) was determined by ^{1}H-NMR (Bruker AVANCE 600 MHz spectrometer, $CDCl_3$

solvent), while the degree of hydrazide functionalization of H-POEGMA (27.5 mol%) was determined by conductometric titration (ManTech Associates) using 50 mg of polymer in 50 mL of 10 mM NaCl as the analyte and 0.1 M NaOH titrant.

2.3 Preparation of CNC Suspensions

CNCs were prepared via sulfuric acid hydrolysis of cotton as described previously.[58] Briefly, Whatman cotton filter paper was submerged in 64 wt% sulfuric acid at 45°C for 45 min, subsequently quenched in DIW, and centrifuged for 10 min at 6000 rpm. The supernatant was decanted, and centrifugation was repeated until a precipitate no longer formed. The cellulose nanocrystal suspension was then dialyzed (MWCO = 12 kDa) in DIW for a minimum of 10 x 12 h cycles. Suspensions were probe sonicated (3 cycles × 15 min, Sonifier 450, Branson Ultrasonics, Danbury, CT), and concentrated by evaporation at ambient conditions. CNCs measured 100 – 200 nm in length by 5 – 12 nm in cross-section as determined by atomic force microscopy (MFP-3D, Asylum Research - Oxford Instruments, Santa Barbara, CA). The sulfate half-ester content of the CNCs was 0.42 wt% (measured via conductometric titration using 100 mg of CNC in 100 mL of 10 mM NaCl as the analysate and 2 mM NaOH as the titrant), and the electrophoretic mobility was -1.86×10^{-8} m^2 V^{-1} s^{-1} (measured on 0.25 wt % CNC suspensions in 10 mM NaCl). CNCs were stored in acid form (pH = 3.2) at 4 °C prior to use.

2.4 Electrospinning POEGMA-CNC Hydrogel Nanofibers

A 5 w/v% solution of PEO (600 kDa) was prepared by dissolving 750 mg of PEO in 15 mL DIW over a period of at least 2 days prior to electrospinning. CNC suspensions were mixed with A-POEGMA or H-POEGMA precursor solutions to yield samples with a POEGMA concentration of 16 wt% and a CNC concentration of 0, 0.2, 1.0, or 1.65 wt%. The resulting POEGMA/CNC suspensions were subsequently mixed with 5 w/v% PEO (1:1

PEO:POEGMA/CNC by volume) to achieve a final concentration of 8 wt% POEGMA, 2.5 w/v% PEO, and 0-0.825 wt% CNC in the electrospinning precursor solutions. The A-POEGMA and H-POEGMA precursor solutions were then loaded into separate compartments of a double-barrel syringe attached to a static mixer and a blunt-tip 18 G needle and mounted in a syringe pump. Electrospinning was conducted using a constant flow rate of 70 nL/min, a distance between the needle tip and collector of 10 cm, and a voltage of 9 kV at room temperature and ambient humidity (between 25 – 35 RH% for each run). Aluminum foil was used to line the electrospinning collector to collect thin samples; for mechanical testing and *in vitro* protein adhesion, aluminum foil was not used as the samples were thick enough to remove without tearing. The collector was optionally rotated at 300 RPM using a rotating drum to prepare electrospun mats with aligned fibers.

2.5 Swelling and Accelerated Degradation

As-prepared electrospun POEGMA-CNC fibers on aluminum foil were cut into ~ 0.5 × 0.5 cm squares and weighed prior to being placed in cell culture inserts and submerged in 2 mL of 10 mM PBS at 37 °C. At each time interval, cell culture inserts were removed, placed on a Kimwipe for 1 min to remove excess PBS, weighed, and refilled with PBS. After initial swelling, the electrospun mats separated from the aluminum foil electrospinning support and were then removed, dried, and weighed. The water content was calculated according to Equation 1, in which the swollen mass is equal to the mass of the wet sample minus the mass of the dry aluminum foil and the mass of the cell culture insert and the dry mass is equal to the mass of initial electrospun mat on the aluminum foil collector minus the mass of the dry aluminum foil.

$$Water\ Content\ \% = \frac{m_{swollen} - m_{dry}}{m_{swollen}} \times 100\% \quad (1)$$

Degradation profiles were determined using the same method as described above but using 1 M HCl instead of 10 mM PBS as the swelling solvent. Samples were allowed to swell initially in 10 mM PBS at 37 °C for 1 hr to enable the delamination of the aluminum foil prior to submerging the mats in 1 M HCl. Electrospun mats were weighed every 2 hours, with solutions replaced after each measurement, until each sample had fully degraded.

2.6 Compression Measurements of Electrospun Mats

Compression measurements were performed on wet POEGMA-CNC electrospun mats in an aqueous environment using a MicroSquisher equipped with a 559-gauge cantilever connected to a 2 × 2 mm stainless steel plate (CellScale Biomaterials Testing, Waterloo, Canada). A 20% strain was used for each cycle with a 30 s ramp and 5 s hold. 3 compression cycles were completed per sample, and a minimum of 4 samples were tested per series. The compressive modulus was determined by calculating the slope of the initial linear region of the generated stress-strain curves. A video showing this technique can be viewed in the Supplementary material.

2.7 Protein Uptake

Fluorescein-isothiocyanate (FITC) labelled bovine serum albumin (BSA) was prepared according to a previously described protocol.[26,55] Briefly, 50 mg of BSA and 1 mg of FITC were added to 100 mL of 10 mM carbonate buffer. The mixture was stirred at room temperature for 12 hours and lyophilized to dryness. A stock solution of 2 mg/mL FITC-BSA was prepared and used immediately to make the required serial dilutions. Electrospun POEGMA-CNC mats were sectioned into 2 × 2 mm samples and allowed to swell in DIW for 1 hour. Samples were then incubated with the prepared FITC-BSA solutions

for 2 hours at 37 °C, after which they were rinsed 3 times with 10 mM PBS prior to measuring the fluorescent signal (Wallac 1420 Explorer Plate Reader, Perkin-Elmer).

2.8 Multi-Scale Structuring of Electrospun POEGMA-CNC Hydrogel Sheets

A CNC-POEGMA hydrogel base layer was first fabricated on a pre-stressed polystyrene substrate according to our previously published protocol.[25] Briefly, A-POEGMA and H-POEGMA copolymer solutions were separately mixed with CNCs at a 5:1 ratio by mass and diluted in DIW to 5.0 wt% POEGMA. Hydrogel base layers were prepared on plasma-cleaned polystyrene substrates (600 mTorr air plasma for 10 minutes, PDC001 Expanded Plasma Cleaner, Harrick Plasma, Ithaca, NY) by spin coating alternating layers of A-POEGMA and H-POEGMA suspensions containing CNCs (G3P spin-coater, Specialty Coating Systems Inc., Indianapolis, IN, USA, 3000 rpm, 7 s acceleration, 30 s dwell). Five deposition cycles were used, with one deposition cycle defined as the sequential spin coating of an A-POEGMA + CNC layer followed by a H-POEGMA + CNC layer.

Following, the hydrogel-coated polystyrene substrates were used as collectors for the electrospinning of POEGMA-CNC nanofibers containing 1.0 wt% CNC using the same electrospinning parameters as previously described. The total time of electrospinning was varied between 10 and 45 minutes to prepare multi-scale structured hydrogels with either a sparse (shorter time) or dense (longer time) fiber layer; an intermediate time of 30 minutes was used for all cell culture experiments. The resulting substrates were shrunk in an isotemp vacuum oven at 130 °C for 15 minutes to create the uniformly structured hydrogel sheets. Biaxial wrinkles were formed by unconstrained shrinking, while uniaxial wrinkles were formed by clamping opposite edges of the substrates to allow shrinking only in one direction (note that wrinkle ridges form in the direction perpendicular to shrinking).

2.9 Cell Metabolic Activity (MTS Assay)

Cell viability and proliferation on hydrogels (unstructured, wrinkled, electrospun, and multi-scale structured) were quantified by an MTS colorimetric assay. Samples were cut, placed in 48-well cell culture plates, sterilized by immersion in 70% ethanol (200 µL) for 30 min, and allowed to dry for one hour under UV light before conditioning overnight in PBS (200 µL). C2C12 cells were seeded onto hydrogel samples at an initial cell density of approximately 10,000 cells/cm^2 and cultured for 3, 5, or 7 days in DMEM containing 10% FBS and 1% penicillin/streptomycin, maintained in a humidified incubator at 37 °C and 5% CO_2. Media was replaced every 2 – 3 days; after culturing, the media was removed followed by the addition of 20 µL of 12 mM MTS solution (final concentration 1.10 mM) and then incubated at 37°C for 2 h. Samples (200 µL) were then transferred to 96-well plates, and the absorbance was recorded at 490 nm by a Tecan M1000 micro-plate reader. Dilutions were performed as necessary to maintain absorbance readings within the calibration range of the dye.

2.10 Confocal Microscopy

To assess cell morphology, hydrogel samples (unstructured, wrinkled, electrospun, and multi-scale structured) were placed in each well of a 24-well glass-bottom plate, upon which C2C12 cells were seeded at an initial cell density of 10,000 cells/cm^2 and cultured for 3 days. Subsequently, the media was removed and 500 µL of prewarmed PBS containing the CFDA SE Cell Tracer (10 µM, Invitrogen) was added to the cells and allowed to incubate for 15 min at 37°C. The CFDA solution was then replaced with fresh, prewarmed culture medium, and the cells were incubated for another 30 min at 37°C. Subsequently, cells were washed with pre-warmed PBS immediately prior to fixing at room temperature for 15 min in 4% paraformaldehyde solution in PBS (500 µL). Following 3 washes in PBS, C2C12 cells were permeabilized with 0.1% Triton X-100 (500 µL) in PBS for 5 min and again washed three times with PBS. The cells were then incubated with 1% BSA in PBS (500 µL) for 30 min at

room temperature to prevent non-specific binding to the multiwell plate. The cells were counterstained with DAPI (300 nM in PBS, 500 µL) for 5 min in the dark and again washed three times with PBS. Samples were examined with a Nikon Eclipse Ti confocal microscope.

2.11 Cell Adhesion and Alignment

To assess cell adhesion and alignment, hydrogel samples were cut and placed in each well of a 24-well plate. Samples were sterilized with 70% ethanol for 30 min, followed by three 20 min long wash cycles in PBS to remove residual ethanol. C2C12 cells were then seeded at an initial cell density of 10,000 cells/cm^2 and cultured for 3 days. Cells were fixed using 2% paraformaldehyde for 15 min and sequentially dehydrated using ethanol solutions of 35%, 50%, 60%, 70%, 80%, 90% (one cycle each of 10 min), and 100% (three cycles of 10 min). The samples were then dried in supercritical conditions to preserve cell morphology and sputter coated with gold (~20 nm thickness). Scanning electron microscopy (SEM, Tecan Vega II LSU Instrument) was subsequently conducted using an operating voltage of 10 kV. For the analysis of electrospun fiber diameter and wrinkle size, ImageJ was used to manually trace and measure the diameter of a minimum of 100 features per image, with a minimum of three images per series analyzed. To determine the cell aspect ratio and orientation angle for cell-laden hydrogel sheets, a minimum of 8 images and 50 total cells were analyzed. Cell aspect ratio was determined by measuring the longest diameter through a given cell and dividing by the perpendicular diameter through the same cell. The angle of the longest diameter through a given cell was used to determine cell orientation, with the resulting cell orientation angles averaged to determine an overall angle deviation. The cell angle deviation was calculated by comparing the cell orientation angle with the average wrinkle orientation angle (the latter calculated by measuring the angle of at least 50 wrinkle segments from mid-point to mid-point) for each cell observed in the SEM image.

2.12 Statistical Methods

For physical property measurements (swelling, compression, degradation, protein adhesion, cell viability), error bars represent the standard deviations of n = 4 independent measurements. ImageJ was used for determining feature sizes and orientations, and unless otherwise noted, error bars represent the standard deviations of n = 100 independent measurements. For cell orientations and ange deviations, at least 50 individual cells were analyzed for each sample. Significant differences (p-values) between independent data sets were assessed using an unpaired t -test.

3. Results

3.1 Electrospinning POEGMA-CNC Hydrogel Nanofibers

To create CNC-impregnated POEGMA hydrogel nanofibers, varying concentrations of CNCs (0.2 – 1.65 wt%) were suspended in solutions of 16 wt% H-POEGMA and A-POEGMA and co-electrospun from a double barrel syringe using PEO as an electrospinning aid. Over the range of CNC concentrations tested, the size and morphology of the resulting electrospun fibers remained consistent, with diameters between 300 and 700 nm (Fig. 1). All tested POEGMA-CNC electrospun mats rapidly reached an equilibrium water content of ~ 98% within one minute upon exposure to 10 mM PBS (Fig. 2A). Both this high water content and the nanofibrous structure of the mats were maintained for up to 30 hours after swelling, albeit with a significant increase in the diameter of the individual fibers (Supplementary material, Fig. S1). Furthermore, all electrospun mats completely degraded in 1 M HCl within 96 hours (i.e., accelerated degradation conditions); across all CNC concentrations tested, peak normalized gel weight was reached at roughly the same time (~8 hours), followed by a steady decrease due to loss of network integrity (Fig. 2B). Note that the variation observed within each group in the degradation plot is typical for degradation experiments on hydrogel nanofibers, in which even small variations in local nanofiber density can significantly change

in-diffusion of the degrading acid; such variations are further compounded by the low density and statics associated with the dry mats that may lead to higher-than-normal weighing variation. Moreover, the compressive modulus of wet POEGMA-CNC electrospun mats increased with increased CNC loading (Fig. 2C), whereby increasing the CNC concentration to 1.65 wt% led to a ~ 2.5 x increase in modulus (up to 25 kPa). Compression curves for each sample can be seen in the Supplementary material, Fig. S2). Finally, increasing the CNC concentration to 1.65 wt% significantly reduced bovine serum albumin protein (BSA) uptake into the electrospun hydrogel mats (Fig. 2D).

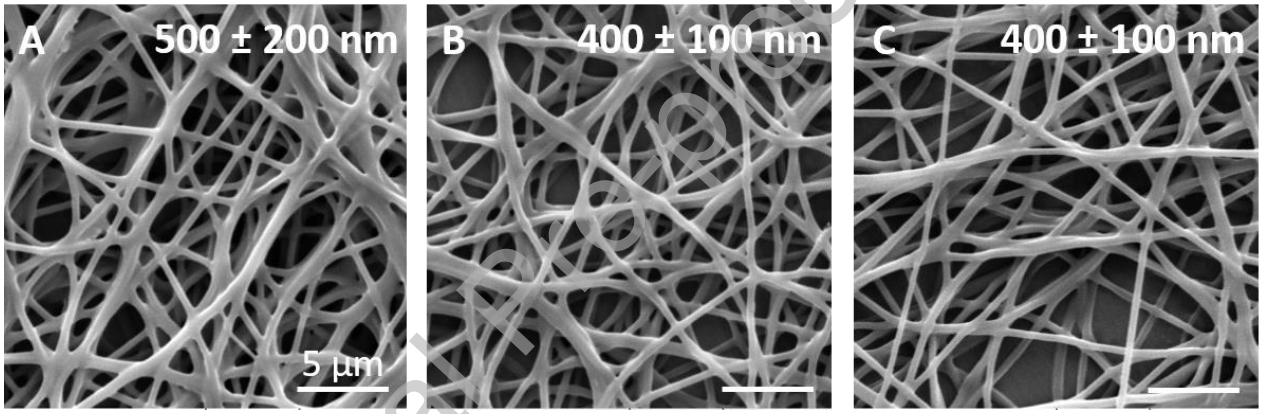

Fig. 1. SEM images and average fiber diameters of electrospun POEGMA-CNC nanofibrous mats containing (A) 0.2, (B) 1.0, or (C) 1.65 wt% CNCs. All scale bars are 5 µm. Inset numbers represent average fiber diameters and standard deviations measured based on ImageJ analysis of n = 100 fibers.

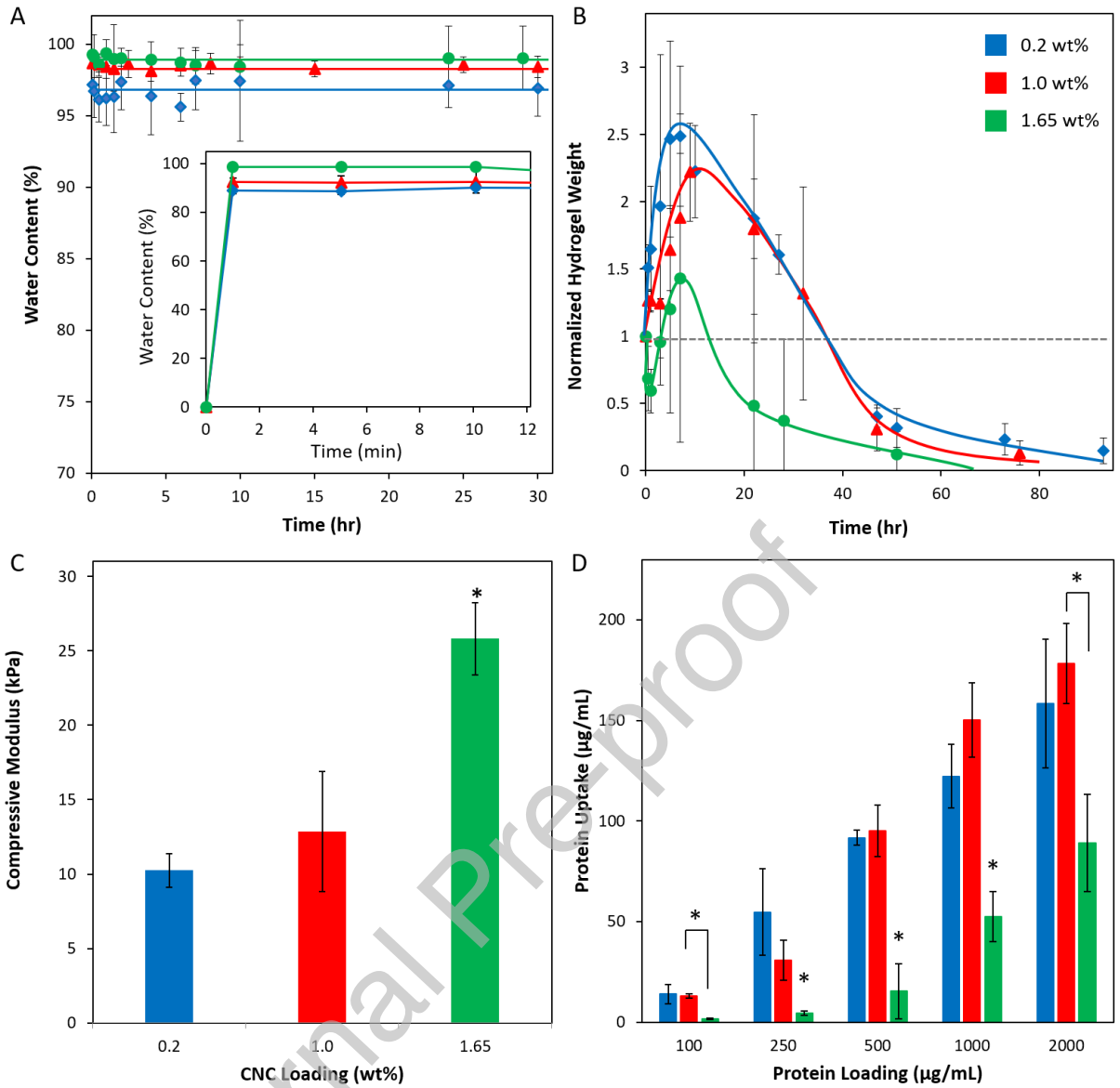

Fig. 2. Physical properties of electrospun POEGMA-CNC nanofibrous mats containing 0.2 (blue), 1.0 (red), or 1.65 (green) wt% CNCs. (A) Swelling profiles in 10 mM PBS at 37 ˚C (inset shows initial time points), (B) accelerated degradation in 1 M HCl at 37 ˚C, (C) compressive modulus in aqueous environment, and (D) BSA uptake following exposure to protein concentrations ranging from 100 - 2000 µg/mL. * = $p < 0.05$. Lines in A and B are guides for the eye.

3.2 Multi-Scale Structuring of Electrospun POEGMA-CNC Hydrogel Sheets

Multi-scale structured hydrogel sheets were prepared using a sequential electrospinning and thermal wrinkling approach (Fig. 3). First, the substrate for thermal wrinkling (prestressed polystyrene) was coated with a thin hydrogel "base layer" of the same composition as the nanofibers. Five sequential deposition cycles (where one deposition cycle = one A-POEGMA (5.0 wt%) + CNCs (1.0 wt%) layer and one H-POEGMA (5.0 wt%) +

CNCs (1.0 wt%) layer) were spin coated onto polystyrene substrates, resulting in a hydrogel sheet of ~1 µm in thickness. Subsequently, the coated polystyrene substrates were positioned on the electrospinning collector and POEGMA-CNC hydrogel nanofibers with the same composition as the base layer were electrospun onto the surface. Note that an overall concentration of 1.0 wt% CNC was chosen for the construction of the hierarchical hydrogel sheets based on our previous study demonstrating that this CNC loading effectively preserved the high fidelity of the nanoscale surface features following thermal wrinkling.[25] Moreover, this also maximizes the fraction of the anti-fibrotic POEGMA polymer at the interface while still enabling hierarchical interface fabrication. The resulting nanofibrous sheets were then subjected to thermal wrinkling at 130 ˚C for 15 minutes to induce wrinkle formation. Electrospun mats deposited directly onto prestressed polystyrene exhibited irregular morphologies upon thermal wrinkling, whereby individual fibers appeared to merge together (Supplementary material, Fig. S3). Of note, the use of a sacrificial photoresist enables the removal of the structured hydrogel sheet from the polystyrene substrate to form a stand-alone structured hydrogel sheet that maintains its wrinkled and fibrous morphology (Supplementary material, Fig. S4); albeit the added thickness of the spin-coated photoresist layer (~ 450 nm) increases the overall sheet thickness and thus the resulting wrinkle size of the hydrogel.

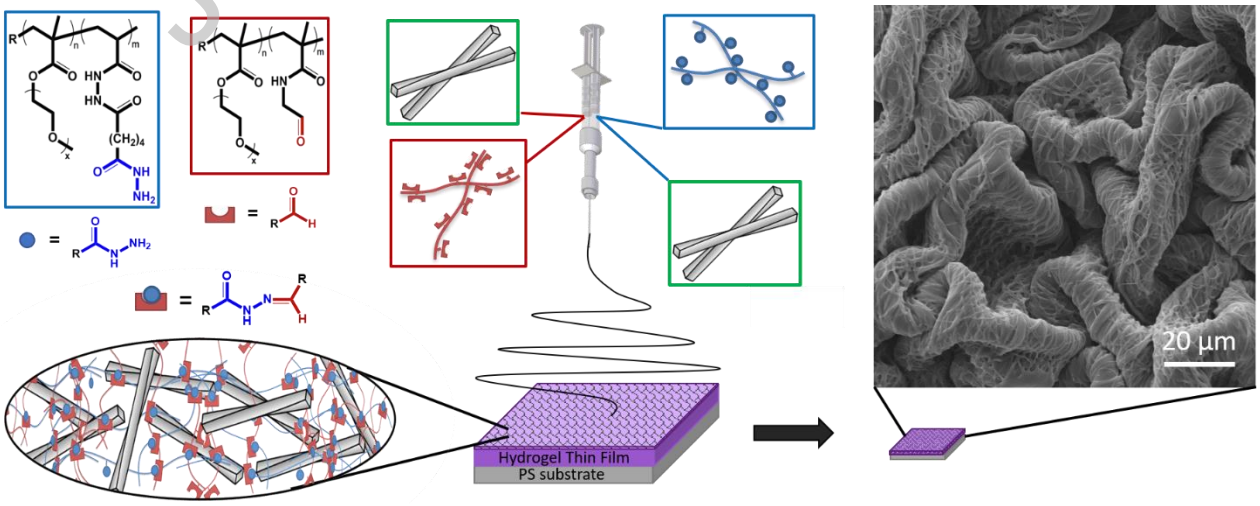

Fig. 3. Schematic representation of the two-step reactive electrospinning and thermal wrinkling process to create multi-scale hierarchically structured POEGMA-CNC hydrogels. Chemical structures for H-POEGMA (blue), A-

POEGMA (red), and hydrazone crosslinking are also depicted. Electrospun mats are collected on a prestressed polystyrene substrate coated with a hydrogel base layer and subsequently thermally wrinkled to create a dual micro-nanostructured interface.

Varying the time of electrospinning, and thus the resulting fiber density on the wrinkled hydrogels, significantly alters the types of wrinkled morphologies generated (Fig. 4; see Supplementary material Fig. S5 for additional images at varying magnifications). Electrospinning for ~ 10 min prior to thermal wrinkling results in a wrinkled surface with sparse fibers, while increasing the electrospinning time to ~ 45 min results in a dense electrospun mat fully covering the underlying hydrogel base layer. Interestingly, hydrogel sheets prepared with a layer of dense electrospun fibers demonstrated a larger wrinkle size than hydrogel sheets prepared with a layer of sparse electrospun fibers (Fig. 4). Of note, electrospinning POEGMA hydrogels alone without CNCs resulted in poor fiber definition after thermal wrinkling (Supplementary material, Fig. S6), likely due to the decreased mechanical strength of the POEGMA-only hydrogels that resulted in high nanofiber deformation in response to the shear induced by thermal wrinkling. As such, the presence of CNCs is essential to create hierarchically-structured 2.5D interfaces.

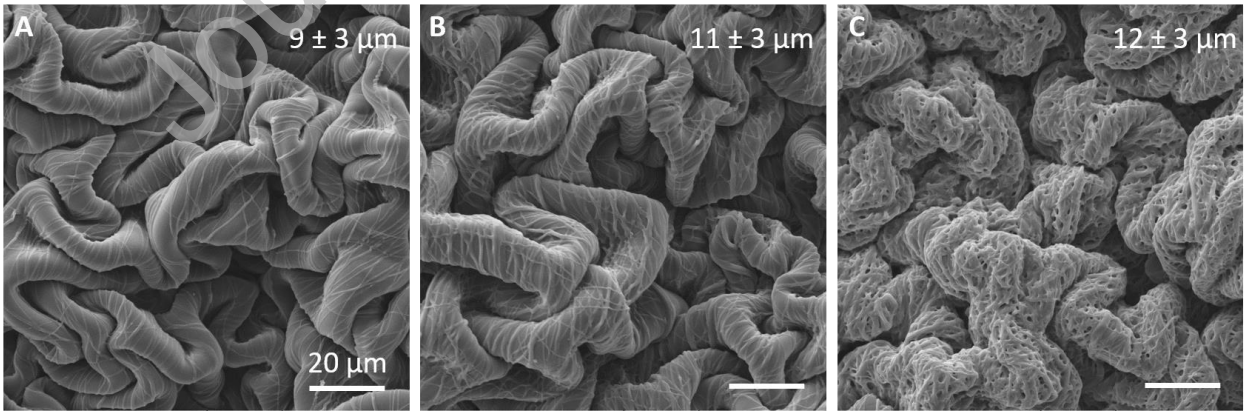

Fig. 4. SEM images of POEGMA-CNC wrinkled electrospun sheets prepared via sequential electrospinning and thermal wrinkling. The fiber density can be tuned by changing the duration of electrospinning from (A) ~ 10 min, (B) ~ 20 min, or (C) ~ 45 min. All scale bars are 20 µm. Inset numbers represent average wrinkle diameters and standard deviations measured based on ImageJ analysis of n = 100 wrinkles.

Uniaxially constraining the geometry of thermal wrinkling in combination with a rotating electrospinning collector (which orients and aligns the deposited nanofibers) enables significantly enhanced control of hydrogel alignment over multiple length scales (Fig. 5A). Using this technique, hierarchically structured hydrogels can be created with optional alignment of both the underlying wrinkles and the overlaying fibers, depending on the direction of nanofiber collection relative to the direction in which the geometry is constrained during the wrinkling step. Here, we define parallel alignment as nanofibers being oriented in the same direction as the wrinkle ridges (Fig. 5B) and perpendicular alignment as nanofibers being oriented across individual wrinkles (Fig. 5C). Interestingly, it was challenging to prepare hydrogel sheets with electrospun fibers oriented parallel to the sheet wrinkles, with the electrospun fibers tending to orient to some degree perpendicularly to the underlying wrinkles regardless of the constraint geometry used. This phenomenon is particularly noticeable in the case of biaxially wrinkled hydrogels (Fig. 4A, B), where nanofibers deposited without a rotating collector (i.e. randomly oriented) were observed to align predominantly perpendicular to the formed wrinkles. Furthermore, although the parallel electrospun/wrinkled hydrogels show a substantial percentage of nanofibers aligned in the wrinkle direction, there is still evidence for some off-axis alignment (Fig. 5B); in contrast, when wrinkling was conducted perpendicular to aligned electrospun nanofibers, virtually no off-axis alignment was observed (Fig. 5C). Additional images of the various prepared hydrogel sheets at varying magnifications are available in the Supplementary material (Fig. S7).

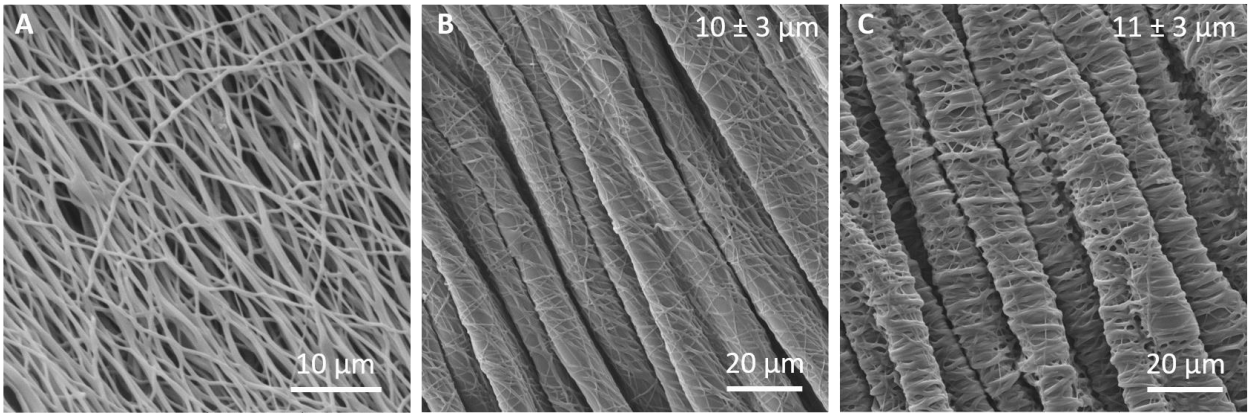

Fig. 5. SEM images of (A) aligned POEGMA-CNC electrospun mats used to prepare uniaxially wrinkled hydrogels with (B) parallel aligned nanofibers (wrinkle ridges parallel to nanofiber alignment), and (C) perpendicular aligned nanofibers (wrinkle ridges perpendicular to nanofiber alignment). Inset numbers represent average wrinkle diameters and standard deviations measured based on ImageJ analysis of n = 100 wrinkles.

3.3 Cell-Biomaterial Interactions in Multi-Scale Structured POEGMA-CNC Hydrogel Sheets

To assess the utility of multi-scale structured POEGMA-CNC wrinkled hydrogels for cell growth applications, C2C12 mouse myoblasts were cultured on biaxially structured electrospun and wrinkled hydrogel sheets and compared to hydrogels of similar composition/chemistry with different morphologies (flat, wrinkled-only, electrospun-only); note that all these interfaces are comprised of hydrogels of the same composition, such that the differences observed can be attributed solely to the morphology of the interface. Over the seven day observation period, cell viability and expansion was similar between the electrospun and biaxially wrinkled hydrogels, biaxially wrinkled hydrogels without an electrospun layer, and hydrogel sheets with no structuring (Fig. 6; see Supplementary material, Fig. S8 for representative images of C2C12 cells after three days of culture). However, cell viability was significantly lower ($p < 0.01$) at the five day time point for electrospun hydrogel mats (without wrinkling) both with and without CNCs.

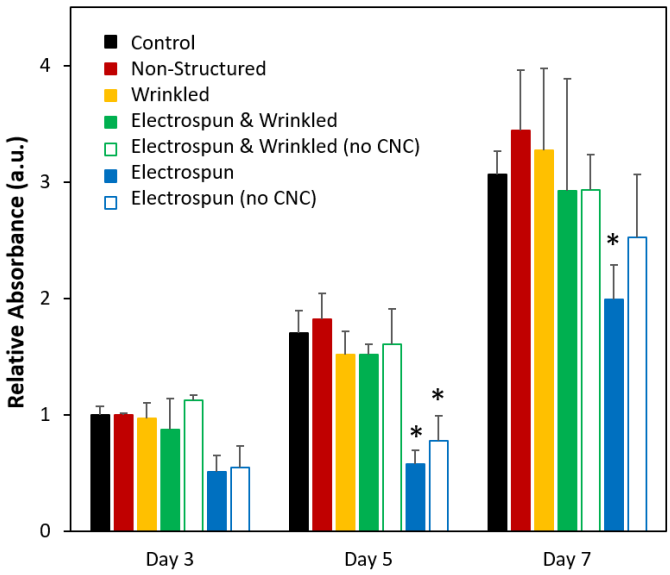

Fig. 6. C2C12 cell expansion on various POEGMA-CNC hydrogel sheets as determined via the MTS assay and normalized to the Day 3 control cultured on tissue culture polystyrene. Note that all samples contain 1.0 wt% CNC. * = $p < 0.01$ compared to the control sample at the same time point.

To assess the effects of the multi-scale and oriented hydrogel sheet morphology on cell alignment, structured hydrogels prepared with various morphologies (i.e., biaxial wrinkles with and without electrospun fibers or uniaxial wrinkles with and without parallel- or perpendicular-oriented electrospun fibers) were seeded with C2C12 cells. The resulting cell orientations on the hydrogel sheets, assessed via SEM, are shown in Fig. 7 (see Supplementary material, Fig. S9 for additional images). In all cases, the wrinkle sizes exhibited a consistent wavelength of ~5 μm (see Supplementary material, Figs. S9 and S10). Biaxially wrinkled hydrogels prepared with no electrospun fibers or randomly oriented electrospun fibers did not elicit any preferential/cooperative alignment of C2C12 cells; however, focal adhesions were apparent in both cases, yielding average cell aspect ratios of 2.1 ± 0.7 and 2.2 ± 1.1 for each respective hydrogel sheet (Supplementary material, Figs. S9 and S10). In comparison, non-wrinkled hydrogel sheets yielded more spherical cell morphologies and smaller cell aspect ratios (1.7 ± 0.4, Supplementary material, Fig. S9). Uniaxially wrinkled hydrogel sheets (regardless of the presence or alignment of electrospun

nanofibers) promoted improved cell alignment and elongation, with C2C12 cells preferentially extending parallel to the underlying wrinkle direction (Fig. 7 and Supplementary material Fig. S9). Correspondingly, the C2C12 cells exhibited a significantly higher aspect ratio on these uniaxially wrinkled sheets, with aspect ratios of 4.5 ± 1.9 μm, 5.2 ± 2.6 μm, and 4.6 ± 2.3 μm measured for uniaxially wrinkled hydrogel sheets with no electrospun fibers, parallel fibers, or perpendicular fibers, respectively. Image analysis of the angle of cell alignment in each case (Fig. 7G – I) also showed clear differences, with the biaxial wrinkled substrates (Fig. 7G) showing a relatively flat distribution of cell orientation angles across a wide angular range while the uniaxial wrinkled substrates (Fig. 7H, I) exhibited a clear maximum at 0° (i.e., cells were preferentially oriented in a given direction).

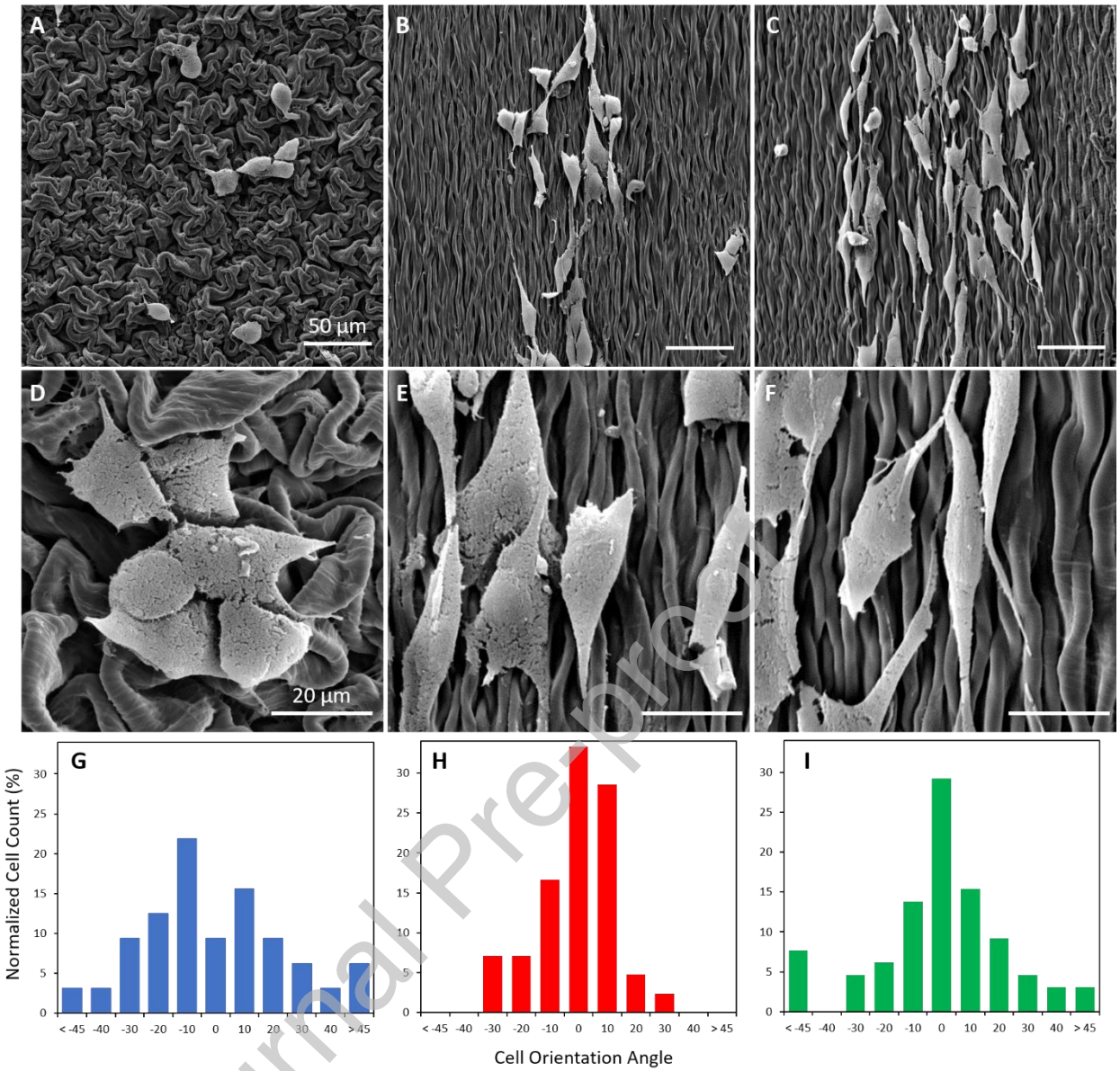

Fig. 7. C2C12 cell adhesion and orientation on electrospun and wrinkled POEGMA-CNC hydrogel sheets. Representative SEM images of (A, D) biaxially wrinkled with unaligned fibers, (B, E) uniaxially wrinkled with parallel-oriented fibers, and (C, F) uniaxially wrinkled with perpendicular-oriented fibers. Scale bars in A – C are 50 µm, and in D – F are 20 µm. (G – I) Histograms of cell orientation angle for cells cultured on the different hydrogel sheets; (G, blue) biaxially wrinkled with unaligned fibers, (H, red) uniaxially wrinkled with parallel-oriented fibers, and (I, green) uniaxially wrinkled with perpendicular-oriented fibers. In each case, at least 50 individual cells were analyzed. Additional SEM images for the replicate samples tested are available in the Supplementary material (Figs. S9, S10, and S11).

Detailed ImageJ analysis of cell orientation with respect to wrinkle direction on the uniaxially wrinkled hydrogel sheets shows more subtle differences depending on the presence and orientation of the electrospun nanofibers (Fig. 8). In all three cases, cells were mostly oriented along the wrinkles; however cells seeded on wrinkled hydrogels with parallel fibers

showed a smaller average deviation in angular alignment relative to the wrinkle direction (12°) compared to cells seeded on wrinkled hydrogels with perpendicular fibers (21°), with the wrinkled hydrogels without an electrospun fiber layer showing intermediate alignment (18°). In addition, the perpendicular nanofiber samples showed a significantly higher population of cells that exhibited high angular variance in their orientation relative to the wrinkle direction (as indicated by the green dots in Fig. 8 at angle deviations of > 60°); in contrast, the parallel wrinkle/nanofiber samples showed only one cell with a misalignment of more than 30°.

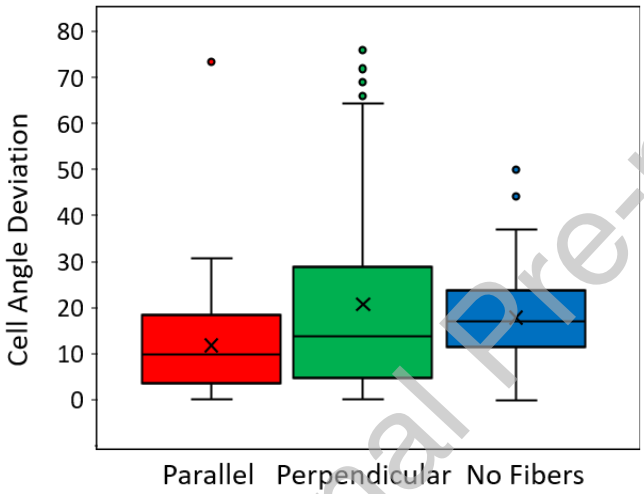

Fig. 8. Box plot showing the deviations of individual cell angles with respect to the average wrinkle orientation on wrinkled hydrogels with parallel oriented fibers (red), perpendicular oriented fibers (green), and no electrospun fibers (blue). In each box, X represents the mean, the midline represents the median, the box represents the interquartile range, and the error bars represent the statistical maximum and minimum values based on the interquartile ranges; the points represent individual cells with angular deviations outside the uncertainty range. In each case, at least 50 individual cells were analyzed.

4. Discussion

POEGMA-CNC hydrogel nanofibers were successfully prepared via electrospinning across all CNC concentrations tested. To ensure effective fiber formation during electrospinning, PEO was used as an electrospinning aid to provide sufficient polymer chain entanglement. As previously demonstrated, the addition of PEO helps prevent droplet/spray formation during electrospinning and can be fully removed from the electrospun hydrogel

matrix by subsequent soaking in water.[12] Note that, due to our desire to match the chemistry of the nanofibers with that of the hydrogel base layer (such that any difference in cell responses could be correlated directly with the morphology of the interface rather than its composition), nanofibers without CNCs were not investigated in detail as they are insufficiently stiff to maintain shape fidelity following thermal wrinkling (Supplementary material, Fig S6). For the CNC concentrations testing, electrospun nanofiber size was relatively unaffected by CNC loading as suspension viscosity and electrospinning parameters were consistent for all formulations.[59] Similarly, given the high porosity of electrospun mats in general, swelling was consistent regardless of CNC concentration, with water rapidly penetrating into the hydrophilic fibrous/macroporous networks. In contrast, hydrogel modulus and network degradation were affected by CNC concentration, as these properties depend strongly on intra-fibrillar interactions; as observed previously in bulk hydrogels, increasing CNC concentration leads to increased physical crosslinking between CNCs and POEGMA and thus increased mechanics and resistance toward hydrolytic degradation.[57] Here, degradation proceeds first by swelling within the individual nanofibers (via the disruption of physical interactions between CNCs and POEGMA) followed by the loss of integrity of the overall scaffold (via the cleavage of POEGMA hydrazone bonds). Expectedly, this initial swelling is hindered for hydrogel mats with 1.65 wt% CNC due to increased physical crosslinking; as the POEGMA concentration (and thus concentration of hydrazone bonds) is similar regardless of CNC concentration, the rate of subsequent hydrolytic degradation is relatively constant across all samples. Finally, protein adsorption was also affected by CNC concentration, whereby increasing CNC concentration to 1.65 wt% led to significantly decreased protein adsorption. This result is consistent with previous observations on bulk hydrogels[55] and can be attributed to the increased adsorption of the POEGMA methacrylate backbone onto the CNCs that assists in orienting the protein-repellent PEG side chains into the protein solution.[57]

When electrospinning was used in combination with thermal wrinkling, multi-scale structured POEGMA-CNC hydrogels were successfully fabricated. Importantly, the use of a hydrogel base layer is necessary to ensure proper adhesion of the electrospun fibers to the polystyrene substrate; the hydrophilic moieties and residual hydrazide/aldehyde groups in the hydrogel base layer facilitate both physical hydrogen bonding/van der Waals interactions and covalent bonding with the deposited electrospun nanofibers to maintain nanofiber shape/conformity during wrinkling. Similarly, the use of CNCs within deposited electrospun fibers is also necessary to maintain nanofiber shape/conformity during wrinkling, due to the increased physical crosslinking between CNCs and POEGMA already discussed above. The deposited electrospun fiber density is increased by lengthening the time of electrospinning; consequently, the underlaying wrinkle size is also increased due to the stiffer overall mechanical properties of the electrospun layer. It has previously been demonstrated that wrinkle size and mechanical properties of the deposited film are positively correlated for wrinkled films.[60,61] Therefore, proper consideration of the mechanical properties of a given material is required for effective utilization of this sequential electrospinning and thermal wrinkling technique.

Hydrogel morphology is independently controlled via the use of a rotating collector to deposit aligned nanofibers. However, it was observed that fibers tend to predominantly align perpendicular to the underlying wrinkles. We hypothesize that the adhesion between the elastic hydrogel nanofibers and the hydrogel base layer works to restrict wrinkling upon heating. As the ability of the electrospun nanofibers to respond to stress is primarily along their length rather than their diameter (due to the chain stretching that occurs during the electrospinning process parallel to fiber direction), nanofibers will primarily orient perpendicular to the direction of wrinkling. Consistent with this hypothesis, hydrogels with perpendicularly aligned fibers show a larger (although not statistically significant) average wrinkle size, consistent with the mechanical properties of the electrospun layer contributing to

the overall ability of the sheet to buckle/wrinkle. Regardless, ordered assemblies of both the nanofibers and the wrinkles to create directionally-controlled multi-scale 2.5D hydrogel sheets can be achieved.

Cell-biomaterial interactions were first investigated by probing C2C12 cell interactions with the structured surfaces, with all hydrogels tested showing cell growth/proliferation between the three and seven day timepoints. Interestingly, the cell viability/growth rate was largely unaffected by changes to hydrogel structuring (flat, wrinkled, or electrospun and wrinkled), with the lower cell viability observed for the electrospun-only samples attributable to the lower modulus of the electrospun mats relative to the other hydrogels.[42,62,63] Subsequent investigations on the effects of sheet morphology on cell orientation and elongation, however, yielded significant differences between the samples; note that wrinkle size was kept constant across samples (on the order of ~ 5 μm), implying that any effect on cell orientation/elongation could be attributed solely to the wrinkle geometry and fiber orientation. Compared to biaxially wrinkled hydrogels, uniaxially wrinkled hydrogels significantly improved cell orientation, with cells elongating in the same direction as the underlying wrinkles as required for the differentiation of C2C12 cells into functional muscle tissue.[43] For uniaxially wrinkled hydrogels, while the wrinkle orientation is the major determinant of cell alignment, nanofiber alignment also significantly impacts cell orientation. Perpendicular nanofibers disorient a significant fraction of cells from aligning along the wrinkle length, while parallel nanofibers aid to reinforce the directionality cues of the micrometer-scale wrinkles. Of note, previous work on electrospinning CNC-based materials has demonstrated CNC alignment along the length of electrospun fibers due to the high shear forces generated during electrospinning;[64–66] as such, any alignment cue from the nanofiber directionality may be also amplified by the internal alignment of anisotropic CNCs within the nanofiber itself. As such, while the microscale wrinkles primarily govern cell alignment, the nanoscale fibers can either reinforce or confuse such directionality cues.

5. Conclusion

In summary, we have demonstrated the fabrication of hierarchically structured electrospun and wrinkled POEGMA-CNC hydrogel sheets that offer exceptional control of hydrogel surface morphology over multiple length scales. While increasing the CNC content of the electrospun mats did not affect the resulting nanofiber size/morphology, it did lead to enhanced mechanical strength and decreased protein adsorption. The electrospun nanofiber orientation and density can both be readily controlled by varying the collector geometry and collection time during electrospinning; independently, wrinkle alignment can be controlled by constraining the substrate during thermal wrinkling. The resulting multi-scale structures and tunable relative alignment of the hydrogel nanofibers and the wrinkles are challenging to achieve using other techniques, which either do not demonstrate the wide range of control over feature size and morphology demonstrated in this work or require complex and tedious fabrication approaches unlike the simple benchtop electrospinning/wrinkling approach used herein. The oriented hydrogel surface structures significantly affected cell alignment, with cells exhibiting a more random orientation on biaxially wrinkled hydrogels but preferentially orienting and extending along wrinkle ridges in uniaxially wrinkled hydrogels. Nanofiber alignment played a supporting role on cell alignment, with parallel-oriented fibers further promoting cell orientation with respect to the underlying uniaxial wrinkle direction while perpendicular-oriented fibers locally de-aligned the cells. We envision that this combined technique of electrospinning and thermal wrinkling may be leveraged to create highly aligned cell scaffolds for both *in vitro* cell screening as well as potential future *in vivo* implants (e.g. muscle regeneration).

Statement of Significance

While structured hydrogels can mimic the morphology of natural tissues, controlling this morphology over multiple length scales remains challenging. Furthermore, the incorporation of secondary morphologies within individual hydrogels via simple manufacturing techniques would represent a significant advancement in the field of structured biomaterials and an opportunity to study complex cell-biomaterial interactions. Herein, we leverage a two-step process based on electrospinning and thermal wrinkling to prepare structured hydrogels with microscale wrinkles and nanoscale fibers. Fiber orientation/density and wrinkle geometry can be independently controlled during the electrospinning and thermal wrinkling processes respectively, demonstrating the flexibility of this technique for creating well-defined multiscale hydrogel structures. Finally, we show that while wrinkle geometry is the major determinant of cell alignment, nanofiber orientation also plays a role in this process.

Declaration of Competing Interest

The authors declare that they have no known competing financial interests or personal relationships that could have appeared to influence the work reported in this paper.

Acknowledgements

K. D. and F. X. contributed equally to this work. Funding from the Natural Sciences and Engineering Research Council of Canada (NSERC, Discovery Grants RGPIN 356609 to T. H., and 402329 to E. C.) is gratefully acknowledged. K. D. acknowledges funding from the NSERC Postdoctoral Fellowship program. J. M. M. is the Tier 2 Canada Research Chair in Micro and Nanostructured Materials, T. H. is the Tier 2 Canada Research Chair in Engineered Smart Materials, and E. C. is the UBC President's Excellence Chair in Forest Bio-Products. This research made use of instrumentation from the Canadian Centre for Electron Microscopy, Brockhouse Institute for Materials Research, and Biointerfaces Institute at McMaster University.

Supplementary materials

Supplementary material associated with this article can be found, in the online version, at

XXX

References

[1] A.S. Hoffman, Hydrogels for biomedical applications, Adv. Drug Deliv. Rev. 54 (2002) 3–12. https://doi.org/10.1016/S0169-409X(01)00239-3.

[2] S. Khetan, J.A. Burdick, Patterning hydrogels in three dimensions towards controlling cellular interactions, Soft Matter. 7 (2011) 830–838. https://doi.org/10.1039/c0sm00852d.

[3] A.K. Gaharwar, N.A. Peppas, A. Khademhosseini, Nanocomposite hydrogels for biomedical applications, Biotechnol. Bioeng. 111 (2014) 441–453. https://doi.org/10.1002/bit.25160.

[4] K.J. De France, F. Xu, T. Hoare, Structured Macroporous Hydrogels: Progress, Challenges, and Opportunities, Adv. Healthc. Mater. 7 (2018) 1700927. https://doi.org/10.1002/adhm.201700927.

[5] A.R. Karimi, A. Khodadadi, Mechanically Robust 3D Nanostructure Chitosan-Based Hydrogels with Autonomic Self-Healing Properties, ACS Appl. Mater. Interfaces. 8 (2016) 27254–27263. https://doi.org/10.1021/acsami.6b10375.

[6] X. Wang, C. Wei, B. Cao, L. Jiang, Y. Hou, J. Chang, Fabrication of Multiple-Layered Hydrogel Scaffolds with Elaborate Structure and Good Mechanical Properties via 3D Printing and Ionic Reinforcement, ACS Appl. Mater. Interfaces. 10 (2018) 18338–18350. https://doi.org/10.1021/acsami.8b04116.

[7] A. Sergeeva, N. Feoktistova, V. Prokopovic, D. Gorin, D. Volodkin, Design of Porous Alginate Hydrogels by Sacrificial CaCO3 Templates: Pore Formation Mechanism, Adv. Mater. Interfaces. 2 (2015) 1500386. https://doi.org/10.1002/admi.201500386.

[8] S. Liu, M. Jin, Y. Chen, H. Gao, X. Shi, W. Cheng, L. Ren, Y. Wang, High internal phase emulsions stabilised by supramolecular cellulose nanocrystals and their application as cell-adhesive macroporous hydrogel monoliths, J. Mater. Chem. B. 5 (2017) 2671–2678. https://doi.org/10.1039/C7TB00145B.

[9] C. Ji, N. Annabi, A. Khademhosseini, F. Dehghani, Fabrication of porous chitosan scaffolds for soft tissue engineering using dense gas CO2, Acta Biomater. 7 (2011) 1653–1664. https://doi.org/10.1016/j.actbio.2010.11.043.

[10] R.Y. Tam, S.A. Fisher, A.E.G. Baker, M.S. Shoichet, Transparent Porous Polysaccharide Cryogels Provide Biochemically Defined, Biomimetic Matrices for Tunable 3D Cell Culture, Chem. Mater. 28 (2016) 3762–3770. https://doi.org/10.1021/acs.chemmater.6b00627.

[11] C.B. Highley, C.B. Rodell, J.A. Burdick, Direct 3D Printing of Shear-Thinning Hydrogels into Self-Healing Hydrogels, Adv. Mater. 27 (2015) 5075–5079. https://doi.org/10.1002/adma.201501234.

[12] F. Xu, H. Sheardown, T. Hoare, Reactive Electrospinning of Degradable Poly(oligoethylene glycol methacrylate)-Based Nanofibrous Hydrogel Networks, Chem. Commun. 52 (2016) 1451–1454. https://doi.org/10.1039/C5CC08053C.

[13] G. Wu, Y. Xia, S. Yang, Buckling, symmetry breaking, and cavitation in periodically micro-structured hydrogel membranes, Soft Matter. 10 (2014) 1392–1399. https://doi.org/10.1039/c3sm51640g.

[14] M. Rizwan, G.S.L. Peh, H.-P. Ang, N.C. Lwin, K. Adnan, J.S. Mehta, W.S. Tan, E.K.F. Yim, Sequentially-crosslinked bioactive hydrogels as nano-patterned substrates with customizable stiffness and degradation for corneal tissue engineering applications, Biomaterials. 120 (2017) 139–154. https://doi.org/10.1016/j.biomaterials.2016.12.026.
[15] A. Castellanos, S.J. Dupont, A.J. Heim, G. Matthews, P.G. Stroot, W. Moreno, R.G. Toomey, Size-exclusion "capture and release" separations using surface-patterned poly(N-isopropylacrylamide) hydrogels, Langmuir. 23 (2007) 6391–6395. https://doi.org/10.1021/la700338p.
[16] T. Yu, C.K. Ober, Methods for the topographical patterning and patterned surface modification of hydrogels based on hydroxyethyl methacrylate, Biomacromolecules. 4 (2003) 1126–1131. https://doi.org/10.1021/bm034079m.
[17] X. Li, M. Guo, F. Wang, X. Shen, Y. Weng, Controllable Hierarchical Surface Patterns of Supramolecular Hydrogels : Harnessing Buckling Instability by Confinement, Chem. - A Eur. J. 23 (2017) 17444–17448. https://doi.org/10.1002/chem.201703155.
[18] M. Gonuguntla, A. Sharma, S.A. Subramanian, Elastic contact induced self-organized patterning of hydrogel films, Macromolecules. 39 (2006) 3365–3368. https://doi.org/10.1021/ma0600411.
[19] S. Kobel, M. Limacher, S. Gobaa, T. Laroche, M.P. Lutolf, Micropatterning of hydrogels by soft embossing, Langmuir. 25 (2009) 8774–8779. https://doi.org/10.1021/la9002115.
[20] P. Kim, D.-H. Kim, B. Kim, S.K. Choi, S.H. Lee, A. Khademhosseini, R.S. Langer, K.-Y. Suh, Fabrication of nanostructures of polyethylene glycol for applications to protein adsorption and cell adhesion, Nanotechnology. 16 (2005) 2420–2426. https://doi.org/10.1088/0957-4484/16/10/072.
[21] B. Chollet, M. Li, E. Martwong, B. Bresson, C. Fretigny, P. Tabeling, Y. Tran, Multiscale Surface-Attached Hydrogel Thin Films with Tailored Architecture, ACS Appl. Mater. Interfaces. 8 (2016) 11729–11738. https://doi.org/10.1021/acsami.6b00446.
[22] S. Kommeren, J. Dongmo, C.W.M. Bastiaansen, R.G. Toomey, R.C. Hayward, A. V. Gorelov, S. Beloshapkin, Y.A. Rochev, Switchable surface structured hydrogel coatings, Soft Matter. 35 (2017) 6377–6383. https://doi.org/10.1039/C7SM00195A.
[23] M. Lei, Y. Gu, A. Baldi, R.A. Siegel, B. Ziaie, High-resolution technique for fabricating environmentally sensitive hydrogel microstructures, Langmuir. 20 (2004) 8947–8951. https://doi.org/10.1021/la048719y.
[24] D. Schmaljohann, M. Nitschke, R. Schulze, A. Eing, C. Werner, K.J. Eichhorn, In situ study of the thermoresponsive behavior of micropatterned hydrogel films by imaging ellipsometry, Langmuir. 21 (2005) 2317–2322. https://doi.org/10.1021/la0476128.
[25] K.J. De France, M. Babi, J. Vapaavuori, T. Hoare, J.M. Moran-Mirabal, E.D. Cranston, 2.5D Hierarchical Structuring of Nanocomposite Hydrogel Films Containing Cellulose Nanocrystals, ACS Appl. Mater. Interfaces. 11 (2019) 6325–6335. https://doi.org/10.1021/acsami.8b16232.
[26] N.M.B. Smeets, E. Bakaic, M. Patenaude, T. Hoare, Injectable poly(oligoethylene glycol methacrylate)-based hydrogels with tunable phase transition behaviours: physicochemical and biological responses., Acta Biomater. 10 (2014) 4143–55. https://doi.org/10.1016/j.actbio.2014.05.035.
[27] J.-F. Lutz, Thermo-Switchable Materials Prepared Using the OEGMA-Platform, Adv. Mater. 23 (2011) 2237–2243. https://doi.org/10.1002/adma.201100597.
[28] E. Bakaic, N.M.B. Smeets, T. Hoare, Injectable hydrogels based on poly(ethylene glycol) and derivatives as functional biomaterials, RSC Adv. 5 (2015) 35469–35486. https://doi.org/10.1039/C4RA13581D.
[29] N.M.B. Smeets, E. Bakaic, M. Patenaude, T. Hoare, Injectable and tunable

poly(ethylene glycol) analogue hydrogels based on poly(oligoethylene glycol methacrylate)., Chem. Commun. 50 (2014) 3306–9. https://doi.org/10.1039/c3cc48514e.
[30] K.J. De France, E.D. Cranston, T. Hoare, Mechanically Reinforced Injectable Hydrogels, ACS Appl. Polym. Mater. 2 (2020) 1016–1030. https://doi.org/10.1021/acsapm.9b00981.
[31] R.M.A. Domingues, M.E. Gomes, R.L. Reis, The potential of cellulose nanocrystals in tissue engineering strategies., Biomacromolecules. 15 (2014) 2327–46. https://doi.org/10.1021/bm500524s.
[32] M. Jorfi, E.J. Foster, Recent advances in nanocellulose for biomedical applications, J. Appl. Polym. Sci. 132 (2015) 41719–41737. https://doi.org/10.1002/app.41719.
[33] D. V Plackett, K. Letchford, J.K. Jackson, H.M. Burt, J. Jackson, H. Burt, A review of nanocellulose as a novel vehicle for drug delivery, Nord. Pulp. Pap. Res. J. 29 (2014) 105–118.
[34] K.J. De France, T. Hoare, E.D. Cranston, Review of Hydrogels and Aerogels Containing Nanocellulose, Chem. Mater. 29 (2017) 4609–4631. https://doi.org/10.1021/acs.chemmater.7b00531.
[35] N. Lin, A. Dufresne, Nanocellulose in biomedicine: Current status and future prospect, Eur. Polym. J. 59 (2014) 302–325. https://doi.org/10.1016/j.eurpolymj.2014.07.025.
[36] F. V. Ferreira, C.G. Otoni, K.J. De France, H.S. Barud, L.M.F. Lona, E.D. Cranston, O.J. Rojas, Porous nanocellulose gels and foams: breakthrough status in the development of scaffolds for tissue engineering, Mater. Today. 37 (2020) 126–141. https://doi.org/10.1016/j.mattod.2020.03.003.
[37] K.J. De France, Z. Zeng, T. Wu, G. Nyström, Functional Materials from Nanocellulose: Utilizing Structure – Property Relationships in Bottom-Up Fabrication, Adv. Mater. (2020) 2000657. https://doi.org/10.1002/adma.202000657.
[38] J.M. Dugan, R.F. Collins, J.E. Gough, S.J. Eichhorn, Oriented surfaces of adsorbed cellulose nanowhiskers promote skeletal muscle myogenesis., Acta Biomater. 9 (2013) 4707–15. https://doi.org/10.1016/j.actbio.2012.08.050.
[39] J.M. Dugan, J.E. Gough, S.J. Eichhorn, Directing the morphology and differentiation of skeletal muscle cells using oriented cellulose nanowhiskers., Biomacromolecules. 11 (2010) 2498–504. https://doi.org/10.1021/bm100684k.
[40] K.J. De France, K.G. Yager, K.J.W. Chan, B. Corbett, E.D. Cranston, T. Hoare, Injectable Anisotropic Nanocomposite Hydrogels Direct in Situ Growth and Alignment of Myotubes, Nano Lett. 17 (2017) 6487–6495. https://doi.org/10.1021/acs.nanolett.7b03600.
[41] H. Aubin, J.W. Nichol, C.B. Hutson, H. Bae, A.L. Sieminski, D.M. Cropek, P. Akhyari, A. Khademhosseini, Directed 3D cell alignment and elongation in microengineered hydrogels, Biomaterials. 31 (2010) 6941–6951. https://doi.org/10.1016/j.biomaterials.2010.05.056.
[42] C.Y. Tay, S.A. Irvine, F.Y.C. Boey, L.P. Tan, Micro- / Nano-engineered Cellular Responses for Soft Tissue Engineering and Biomedical Applications, Small. 7 (2011) 1361–1378. https://doi.org/10.1002/smll.201100046.
[43] Y. Li, G. Huang, X. Zhang, L. Wang, Y. Du, T.J. Lu, F. Xu, Engineering cell alignment in vitro, Biotechnol. Adv. 32 (2014) 347–365. https://doi.org/10.1016/j.biotechadv.2013.11.007.
[44] C. Zhou, J. Zhao, S. Saem, U. Gill, H.D.H. Stover, J.M. Moran-Mirabal, Self-Cross-Linking p(APM-co-AA) Microstructured Thin Films as Biomimetic Scaffolds, ACS Appl. Bio Mater. 1 (2018) 1512–1522. https://doi.org/10.1021/acsabm.8b00424.
[45] P. Linke, R. Suzuki, A. Yamamoto, M. Nakahata, M. Kengaku, T. Fujiwara, T. Ohzono, M. Tanaka, Dynamic Contact Guidance of Myoblasts by Feature Size and Reversible

Switching of Substrate Topography: Orchestration of Cell Shape, Orientation, and Nematic Ordering of Actin Cytoskeletons, Langmuir. 35 (2019) 7538–7551. https://doi.org/10.1021/acs.langmuir.8b02972.

[46] T. Jiang, E.J. Carbone, K.W.H. Lo, C.T. Laurencin, Electrospinning of polymer nanofibers for tissue regeneration, Prog. Polym. Sci. 46 (2015) 1–24. https://doi.org/10.1016/j.progpolymsci.2014.12.001.

[47] F. Xu, M. Dodd, H. Sheardown, T. Hoare, Single-Step Reactive Electrospinning of Cell-Loaded Nanofibrous Scaffolds as Ready-to-Use Tissue Patches, Biomacromolecules. 19 (2018) 4182–4192. https://doi.org/10.1021/acs.biomac.8b00770.

[48] A. Komez, E.T. Baran, U. Erdem, N. Hasirci, V. Hasirci, Construction of a patterned hydrogel-fibrous mat bilayer structure to mimic choroid and Bruch's membrane layers of retina, J. Biomed. Mater. Res. - Part A. 104A (2016) 2166–2177. https://doi.org/10.1002/jbm.a.35756.

[49] K. Tonsomboon, M.L. Oyen, Composite electrospun gelatin fiber-alginate gel scaffolds for mechanically robust tissue engineered cornea, J. Mech. Behav. Biomed. Mater. 21 (2013) 185–194. https://doi.org/10.1016/j.jmbbm.2013.03.001.

[50] N.F. Huang, S. Patel, R.G. Thakar, J. Wu, B.S. Hsiao, B. Chu, R.J. Lee, S. Li, Myotube assembly on nanofibrous and micropatterned polymers, Nano Lett. 6 (2006) 537–542. https://doi.org/10.1021/nl060060o.

[51] N. Narayanan, C. Jiang, G. Uzunalli, S.K. Thankappan, C.T. Laurencin, M. Deng, Polymeric Electrospinning for Musculoskeletal Regenerative Engineering, Regen. Eng. Transl. Med. 2 (2016) 69–84. https://doi.org/10.1007/s40883-016-0013-8.

[52] K.J. Aviss, J.E. Gough, S. Downes, Aligned Electrospun Polymer Fibres for Skeletal Muscle Regeneration, Eur. Cells Mater. 19 (2010) 193–204.

[53] J. Zhong, H. Zhang, J. Yan, X. Gong, Effect of nanofiber orientation of electrospun nanofibrous scaffolds on cell growth and elastin expression of muscle cells, Colloids Surfaces B Biointerfaces. 136 (2015) 772–778. https://doi.org/http://dx.doi.org/10.1016/j.colsurfb.2015.10.017.

[54] T. Or, S. Saem, A. Esteve, D.A. Osorio, K.J. De France, J. Vapaavuori, T. Hoare, A. Cerf, E.D. Cranston, J.M. Moran-Mirabal, Patterned Cellulose Nanocrystal Aerogel Films with Tunable Dimensions and Morphologies as Ultra-Porous Scaffolds for Cell Culture, ACS Appl. Nano Mater. 2 (2019) 4169–4179. https://doi.org/10.1021/acsanm.9b00640.

[55] K.J. De France, M. Badv, J. Dorogin, E. Siebers, V. Panchal, M. Babi, J.M. Moran-Mirabal, M. Lawlor, E.D. Cranston, T. Hoare, Tissue Response and Biodistribution of Injectable Cellulose Nanocrystal Composite Hydrogels, ACS Biomater. Sci. Eng. 5 (2019) 2235–2246. https://doi.org/10.1021/acsbiomaterials.9b00522.

[56] M. Chau, K.J. De France, B. Kopera, V.R. Machado, S. Rosenfeldt, L. Reyes, K.J.W. Chan, S. Förster, E.D. Cranston, T. Hoare, E. Kumacheva, Composite hydrogels with tunable anisotropic morphologies and mechanical properties, Chem. Mater. 28 (2016) 3406–3415. https://doi.org/10.1021/acs.chemmater.6b00792.

[57] K.J. De France, K.J.W. Chan, E.D. Cranston, T. Hoare, Enhanced mechanical properties in cellulose nanocrystal-poly(oligo ethylene glycol methacrylate) injectable nanocomposite hydrogels through control of physical and chemical cross-linking, Biomacromolecules. 17 (2016) 649–660. https://doi.org/10.1021/acs.biomac.5b01598.

[58] S. Beck-Candanedo, M. Roman, D.G. Gray, Effect of Reaction Conditions on the Properties and Behavior of Wood Cellulose Nanocrystal Suspensions, Biomacromolecules. 6 (2005) 1048–1054. https://doi.org/10.1021/bm049300p.

[59] Z.M. Huang, Y.Z. Zhang, M. Kotaki, S. Ramakrishna, A review on polymer nanofibers by electrospinning and their applications in nanocomposites, Compos. Sci. Technol. 63

(2003) 2223–2253. https://doi.org/10.1016/S0266-3538(03)00178-7.
[60] J.Y. Chung, A.J. Nolte, C.M. Stafford, Surface wrinkling: A versatile platform for measuring thin-film properties, Adv. Mater. 23 (2011) 349–368. https://doi.org/10.1002/adma.201001759.
[61] U. Gill, T. Sutherland, S. Himbert, Y. Zhu, M.C. Rheinstädter, E.D. Cranston, J.M. Moran-Mirabal, Beyond buckling: humidity-independent measurement of the mechanical properties of green nanobiocomposite films, Nanoscale. 9 (2017) 7781–7790. https://doi.org/10.1039/C7NR00251C.
[62] L. Wang, C. Wang, S. Wu, Y. Fan, X. Li, Influence of the mechanical properties of biomaterials on degradability, cell behaviors and signaling pathways: Current progress and challenges, Biomater. Sci. 8 (2020) 2714–2733. https://doi.org/10.1039/d0bm00269k.
[63] K.G. Robinson, T. Nie, A.D. Baldwin, E.C. Yang, K.L. Kiick, R.E. Akins, Differential effects of substrate modulus on human vascular endothelial, smooth muscle, and fibroblastic cells, J. Biomed. Mater. Res. - Part A. 100 A (2012) 1356–1367. https://doi.org/10.1002/jbm.a.34075.
[64] S. Huan, G. Liu, W. Cheng, G. Han, L. Bai, Electrospun Poly(lactic acid)-Based Fibrous Nanocomposite Reinforced by Cellulose Nanocrystals: Impact of Fiber Uniaxial Alignment on Microstructure and Mechanical Properties, Biomacromolecules. 19 (2018) 1037–1046. https://doi.org/10.1021/acs.biomac.8b00023.
[65] N.D. Wanasekara, R.P.O. Santos, C. Douch, E. Frollini, S.J. Eichhorn, Orientation of cellulose nanocrystals in electrospun polymer fibres, J. Mater. Sci. 51 (2016) 218–227. https://doi.org/10.1007/s10853-015-9409-y.
[66] X. He, Q. Xiao, C. Lu, Y. Wang, X.X. Zhang, J. Zhao, W. Zhang, X.X. Zhang, Y. Deng, Uniaxially Aligned Electrospun All-Cellulose Nanocomposite Nano fibers Reinforced with Cellulose Nanocrystals: Scaffold for Tissue Engineering, Biomacromolecules. 15 (2014) 618–627. https://doi.org/10.1021/bm401656a.

Graphical Abstract